Journal of Catalysis **193,** 88–95 (2000)
doi:10.1006/jcat.2000.2833, available online at http://www.idealibrary.com on IDEAL®

A Study on the Dispersion of NiO and/or WO_3 on Anatase

Bin Xu, Lin Dong, Yining Fan, and Yi Chen[1]

Department of Chemistry, Institute of Mesoscopic Solid State Chemistry, Nanjing University, Nanjing 210093, China

Received November 15, 1999; accepted January 28, 2000

A series of anatase-supported NiO and/or WO_3 samples are prepared by impregnation and characterized by various experimental methods. The results reveal that for the anatase-supported single oxide samples, nickel oxide and tungsten oxide can be highly dispersed on the surface of the support with a dispersion capacity of 6.65 and 4.85 cations/nm^2 of anatase, respectively; the experimental data are consistent with the incorporation model proposed earlier by the authors. For the supported binary oxide samples, i.e., NiO/WO_3–TiO_2, WO_3/NiO–TiO_2, and NiO–WO_3/TiO_2 samples, XRD, TPR, Raman, and UV-DRS results have suggested that the dispersion state of oxides is strongly related to the loading sequence of the individual metal oxides.

Key Words: **WO_3; NiO; TiO_2; dispersion; interaction.**

INTRODUCTION

Supported metal oxides have been extensively used as total or partial oxidation catalysts or as the precursors of supported metal or sulfide catalysts that are widely applied in many chemical processes. It has been well established that the properties of the active species of the catalysts are often strongly influenced by the support. Accordingly, a large number of studies have been devoted to exploring the interaction between the support and the dispersed oxide species, and various explanations or models concerning the nature of the interaction have been proposed (1–4).

Supported NiO and WO_3 catalysts are known for catalyzing different important reactions, e.g., NiO/Al_2O_3 for CO methanation (5) and N_2O decomposition (6), WO_3/Al_2O_3 for propene metathesis (7), WO_3/SiO_2 for olefin disproportionation (8), and WO_3/Fe_2O_3 for the reduction of NO_x in combustion flue gases (9). Supported NiO–WO_3 samples deserve attention as they are the precursors of the widely used hydrodesulfurization (HDS) (10), hydrogenation (11), and hydrocracking (12) catalysts. Although under HDS reaction conditions the catalysts are being changed to sulfide to a large extent, it is relevant to study their oxide precursors as it has been reported that there are some direct relationships between the properties of the oxide precursors and the corresponding sulfide catalysts (13). It is expected that hydrogenation and hydrocracking reactions will become more important due to the need to produce clean fossil fuels from heavy petroleum fractions and coal. In fact, there is a great demand for catalysts having better properties for the hydrogenation of the heavy fraction of petroleum and of coal as well as coal-derived liquids. In these respects, W-based catalysts have been reported to be better than Mo-based catalysts (12, 14), although fewer studies have been conducted on the W-based catalysts (15–18).

Titanium oxide is one of the major supports widely applied in heterogeneous catalysis (19), and it has been found that the catalytic activity of HDS catalyst can be improved by choosing titanium oxide instead of γ-Al_2O_3 as the support (20, 21). To investigate the interactions among the oxide species in anatase-supported single oxide and binary oxide systems, a series of anatase-supported NiO and/or WO_3 samples have been prepared by the impregnation method and characterized by X-ray diffraction (XRD), X-ray photoelectron spectroscopy (XPS), temperature-programmed reduction (TPR), ultraviolet diffuse reflectance spectroscopy (UV-DRS), and Fourier transform Raman spectroscopy (FT-LRS). The results have shown that the dispersion capacity of NiO or WO_3 on anatase is consistent with the value expected on the basis of the incorporation model reported elsewhere (4), and the surface states of the supported binary oxide samples are strongly dependent on the loading sequence of the individual oxides.

METHODS

Sample Preparation

The anatase support was prepared by the hydrolysis of $Ti(SO_4)_2$ (A.R.) with aqueous ammonia, and the product was washed, dried, and calcined at 873 K for 3 h. The BET surface area of the support was 51 m^2/g. The titania thus prepared was verified to have the crystalline form of anatase by XRD (Fig. 1a) and denoted as TiO_2 in this paper.

The NiO/TiO_2 and WO_3/TiO_2 samples were prepared by impregnating the TiO_2 support with aqueous solutions containing the required amount of $Ni(NO_3)_2 \cdot 6H_2O$ (A.R.) and

[1] To whom correspondence should be addressed. Fax: 0086-025-3317761. E-mail: chenyi@nju.edu.cn.

0021-9517/00 $35.00

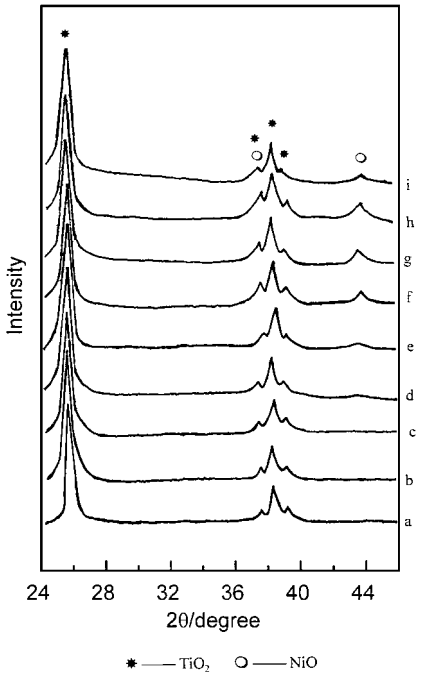

FIG. 1. XRD patterns of the anatase support (a), and the NiO/TiO_2 samples (b–h): (b) Ni(2.9)/TiO_2, (c) Ni(5.9)/TiO_2, (d) Ni(7.2)/TiO_2, (e) Ni(8.8)/TiO_2, (f) Ni(11.9)/TiO_2, (g) Ni(14.5)/TiO_2, and (h) Ni(18.3)/TiO_2. Sample (i) is a physical mixture of NiO and anatase corresponding to an NiO content of 3.0 Ni^{2+}/nm^2 of TiO_2.

ammonia tungstate, respectively. The NiO–WO_3/TiO_2 samples were prepared by impregnating the TiO_2 support with aqueous solutions consisting of a mixture containing the required amount of ammonia tungstate and $Ni(NO_3)_2 \cdot 6H_2O$ (A.R.). The impregnated products were dried at 383 K overnight, hand ground in an agate mortar, and then calcined in air at 773 K for 3 h. The NiO/WO_3–TiO_2 and WO_3/NiO–TiO_2 samples were prepared by impregnating the required amount of $Ni(NO_3)_2 \cdot 6H_2O$ (A.R.) or ammonia tungstate, respectively, on the modified supports, i.e., on WO_3–TiO_2 and NiO–TiO_2, which were prepared according to the procedures mentioned above. The samples were then dried and calcined under the conditions given above. Samples with various loading amounts of Ni^{2+} and W^{6+} (expressed in ions/nm^2) on anatase were prepared, and their compositions were denoted by the data in the parentheses right next to the symbol of the element, e.g., Ni(6.0)/W(3.0)-TiO_2 means the loading amounts of Ni^{2+} and W^{6+} were 6.0 and 3.0 ions/nm^2 of TiO_2, respectively.

Instrumental

XRD was carried out with a Shimadzu XD-3A diffractometer employing Ni-filtered Ni$K\alpha$ radiation ($\lambda =$ 0.15418 nm). The X-ray tube was operated at 35 kV and 15 mA.

XPS results were obtained by using a V. G. Escalab MK II spectrometer equipped with a hemispherical electron analyzer. The spectrometer was operated at 13 kV and 20 mA using a magnesium anode (Mg$K\alpha$, $\lambda = 1254.6$ eV). C1*s* (284.6 eV) was used as reference for the calculation of the measured binding energies.

UV-DRS measurements were carried out on a Shimadzu UV-2100 spectrometer equipped with a diffuse reflectance accessory with an integrating sphere, and $BaSO_4$ powder was used as reference.

FT-Raman spectra were recorded on a Bruker RFS 100 spectrometer with an InGaAs detector cooled by liquid nitrogen. Raman excitation at 1064 nm provided by a Na:YAG laser was used for excitation. The laser power applied at the sample was 100 mW, and the wavenumber accuracy was 4 cm^{-1}.

For TPR measurements, prior to the reduction about 40 mg sample in a quartz U-tube reactor was pretreated in a nitrogen stream at 373 K for 1 h and cooled down to room temperature. The temperature was then increased linearly at a rate of 8 $K \cdot min^{-1}$ under a flowing H_2-N_2 mixture (15% H_2 by volume) of 30 $ml \cdot min^{-1}$. The consumption of H_2 was detected by an online thermal conductivity detector.

RESULTS AND DISCUSSION

Characterization of the NiO/TiO_2 Samples

The XRD patterns of the NiO/TiO_2 samples with various NiO loadings are shown in Fig. 1. No peaks corresponding to the crystalline phase of NiO were observed in samples with low NiO loadings (profiles b and c of Fig. 1). However, when the NiO loading is increased across a borderline, i.e., above its dispersion capacity, the characteristic peaks of crystalline NiO show up clearly (Figs. 1d–1h). A physical mixture of crystalline NiO and the anatase support corresponding to an NiO content of 3.0 Ni^{2+}/nm^2 (TiO_2) is presented for comparison, in which the peaks of the crystalline NiO can be seen clearly (Fig. 1i). XRD quantitative analysis result demonstrates that with the increase of the loading amount of nickel oxide on anatase a highly dispersed surface species is formed at first, and the crystalline NiO shows up finally; since then the intensities of the characteristic peaks of NiO crystalline increase linearly with the increase of the NiO content in the sample.

The dispersion capacities of the supported metal oxides are measured by methods suggested in the literature (3). As shown in Fig. 2, the dispersion capacity of NiO on anatase is evaluated to be 6.65 Ni^{2+}/nm^2 of TiO_2 by extrapolating the above straight line to get the intercept on abscissa.

The DRS results of the NiO/TiO_2 samples are listed in Table 1. Only the absorption bands between 400 and 800 nm are discussed because the anatase support has strong absorption bands to produce interference below 400 nm. As can be seen from the table there is an absorption band at ~665 nm for all the samples, and when the loading amount

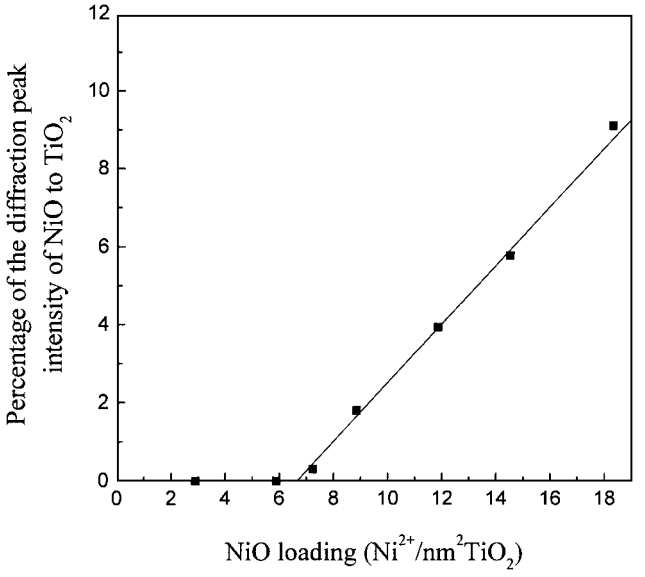

FIG. 2. XRD peak intensity ratio of NiO to TiO_2 vs NiO content in the NiO/TiO_2 samples.

of NiO exceeds its dispersion capacity on anatase, another band around 725 nm shows up, indicating the appearance of crystalline NiO (15, 22–24). Taking into consideration of the XRD results, the band around 665 nm is attributed to the dispersed nickel oxide species. Noticeably, it has been reported that NiO in MgO has an absorption band at 671 nm resulting from the *d–d* transition of the octahedrally coordinated Ni^{2+} ions (25), which is consistent with the above experimental result. As will be discussed later, according to the incorporation model the dispersed Ni^{2+} ions on the surface of anatase should most probably be octahedrally coordinated.

Characterization of the WO_3/TiO_2 Samples

The XRD profiles of WO_3/TiO_2 samples with various W^{6+} loadings are shown in Fig. 3, from which the dispersion capacity of WO_3 on anatase is determined to be 4.85 W^{6+}/nm^2 of TiO_2 as shown in Fig. 4. Similar to the results discussed in the NiO/TiO_2 system, crystalline WO_3 can be detected only on the surface of those samples in which the

TABLE 1

DRS Data of the NiO/TiO_2 and $NiO\text{-}WO_3/TiO_2$ Samples

Sample	Wavelength (nm)	
$Ni(2.9)/TiO_2$	~665	
$Ni(8.8)/TiO_2$	~665	~725
$Ni(11.9)/TiO_2$	~665	~725
$Ni(14.5)/TiO_2$	~665	~725
$Ni(3.1)\text{-}W(6.0)/TiO_2$	~470	~665
$Ni(6.0)\text{-}W(3.1)/TiO_2$	~470	~665
$Ni(3.6)\text{-}W(3.7)/TiO_2$	~470	~665

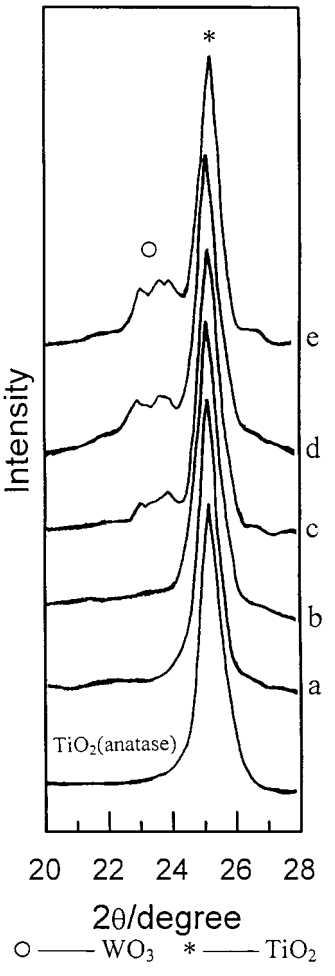

FIG. 3. XRD patterns of the WO_3/TiO_2 samples: (a) $W(3.0)/TiO_2$, (b) $W(4.8)/TiO_2$, (c) $W(7.4)/TiO_2$, (d) $W(10.9)/TiO_2$, and (e) $W(15.1)/TiO_2$.

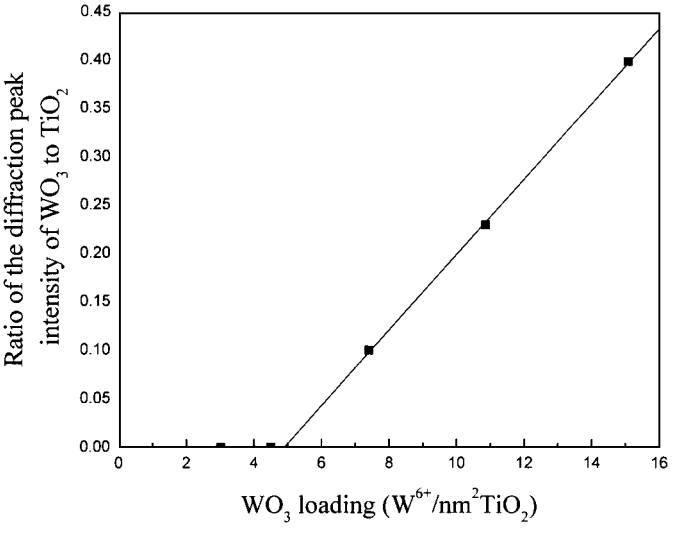

FIG. 4. XRD peak intensity ratio of WO_3 to TiO_2 vs WO_3 content in the WO_3/TiO_2 samples.

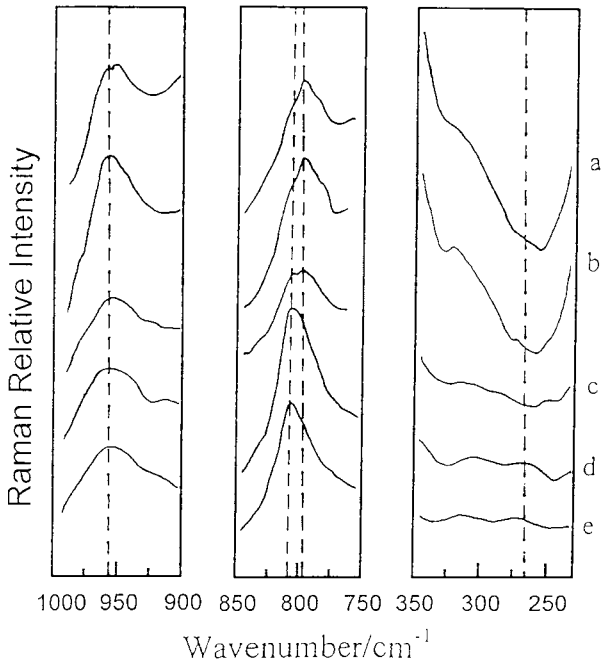

FIG. 5. Raman spectra of the WO_3/TiO_2 samples: (a) W(3.0)/TiO_2, (b) W(4.8)/TiO_2, (c) W(7.4)/TiO_2, (d) W(10.9)/TiO_2, and (e) W(15.1)/TiO_2.

loading amount of WO_3 exceeds its dispersion capacity on anatase.

Raman spectra of the WO_3/TiO_2 samples are shown in Fig. 5. For samples with WO_3 loading below its dispersion capacity, i.e., (a) W(3.0)/TiO_2 and (b) W(4.8)/TiO_2, two peaks at ~970 and ~794 cm^{-1} are observed. The peak around 794 cm^{-1} is attributed to the weak TiO_2 (anatase) transition (26, 27), while the peak at ~970 cm^{-1} is attributed to the symmetrical W═O stretching mode of the dispersed tungsten oxide species on the surface of the anatase (26, 27). For the samples with WO_3 loading beyond its dispersion capacity, i.e., (c) W(7.40)/TiO_2, (d) W(10.9)/TiO_2, and (e) W(15.1)/TiO_2, another peak at 808 cm^{-1} assigned to the W–O stretching mode (28) clearly shows up, indicating the existence of crystalline WO_3, which has three characteristic peaks around 808, 719, and 276 cm^{-1} (18, 26–30). With the increasing of the loading amount of WO_3, finally the peak at ~794 cm^{-1} is overwhelmed by the peak at ~808 cm^{-1}, as shown in Figs. 5d and 5e. For the W(10.9)/TiO_2 and W(15.1)/TiO_2 samples, a Raman band at ~276 cm^{-1} associated with the W–O–W deformation of the crystalline WO_3 (29) can also be detected, but its intensity is apparently lower than that of the peak at ~808 cm^{-1}. In our cases, the Raman band at 719 cm^{-1} for crystalline WO_3 cannot be detected, as it is overlapped by a very intensive Raman band of TiO_2 at ~643 cm^{-1} (26).

The W4$f_{7/2}$, Ti2$p_{3/2}$, and O1s binding energies of the WO_3/TiO_2 samples are listed in Table 2. It is evident that the oxidation state of tungsten ions in all the samples is W^{6+} (31); however its binding energy (W4f) decreases with the increasing of the WO_3 content until a value of 35.4 eV is reached, which is close to the binding energy of pure WO_3 (35.5 eV). The results reveal the fact that when tungsten oxide is highly dispersed on the surface of anatase, the binding energy of the dispersed species is somewhat larger than that of pure WO_3 due to the interaction between anatase and the supported tungsten species. By increasing the loading amount of WO_3, with the presence of the bulk phase WO_3, the binding energy of the supported species finally approaches the value of pure WO_3. Similar phenomena have been observed by Billoen and Pott in their study on WO_3/Al_2O_3 samples; an interaction between the WO_3 and the alumina support has been suggested (32).

TABLE 2

XPS Binding Energies of WO_3 and the WO_3/TiO_2 Samples

Sample	Binding energy (eV)		
	W4$f_{7/2}$	Ti2$p_{3/2}$	O1s
W(3.0)/TiO_2	35.8	458.6	530.0
W(4.8)/TiO_2	36.0	458.9	530.2
W(7.4)/TiO_2	35.6	458.7	530.1
W(10.9)/TiO_2	35.4	458.6	529.9
W(15.1)/TiO_2	35.4	458.3	529.7
WO_3	35.5		530.3

It has been well established that the XPS intensity ratios of metal cations of the metal oxide to the metal cations of the oxide support can provide important information regarding the dispersion and crystallite size of supported metal particles (3, 31, 33, 34). The relationship between the W4d/Ti2p ratio and WO_3 content of the WO_3/TiO_2 samples is shown in Fig. 6 (for these experiments, the strongest XPS

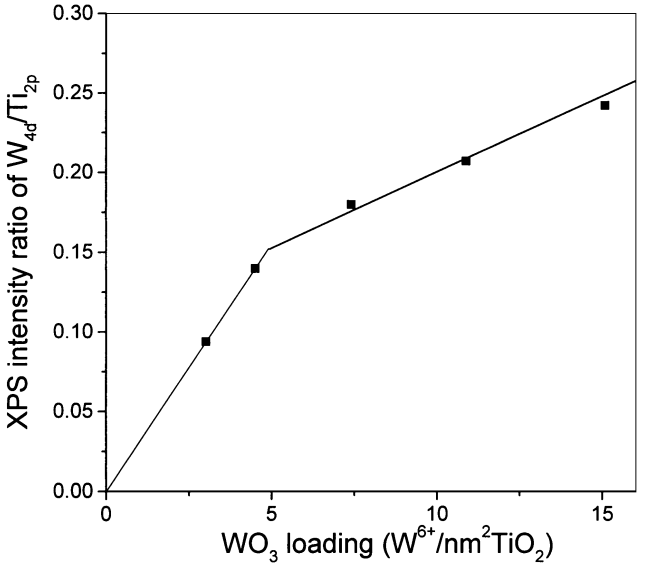

FIG. 6. XPS peak intensity ratio of W4d/Ti2p vs WO_3 content in the WO_3/TiO_2 samples.

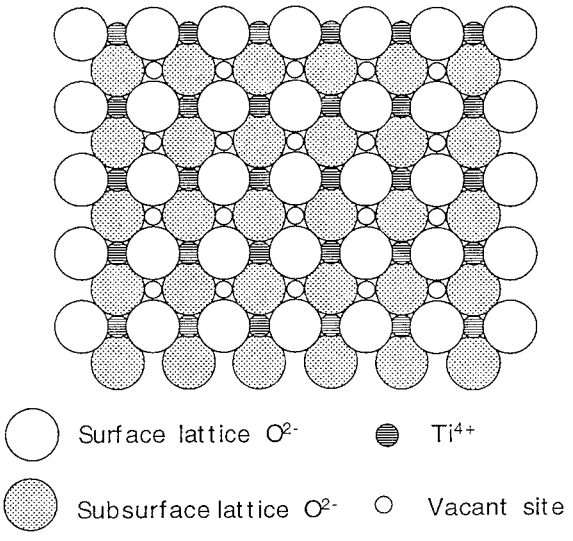

FIG. 7. The (001) plane of anatase.

peak of WO_3, i.e., W4*f*, cannot be measured quantitatively as it is overlapped by peak Ti3*p*). As shown in Fig. 6, there are two straight lines with different slopes corresponding respectively to samples with WO_3 loading lower and higher than its dispersion capacity, and from the intercept of the two lines one can estimate the dispersed capacity of WO_3 on anatase to be 4.9 W^{6+}/nm^2 of TiO_2, in good agreement with the value obtained from XRD quantitative analysis.

The above results are consistent with the incorporation model proposed by Chen *et al.* and reported elsewhere (4, 34–38). Taking into consideration that the (001) plane is preferentially exposed on the surface of anatase (1, 39), as shown in Fig. 7, the vacant site density on the surface of anatase is 6.98 site/nm^2 of TiO_2 (38). Each of the vacant sites has five neighboring lattice oxygen anions and would become octahedrally coordinated by adding one O^{2-} on the top. The dispersion capacity of NiO on anatase is expected to be 6.98 Ni^{2+}/nm^2 (TiO_2) as according to the model each incorporated Ni^{2+} ion is accompanied by only one O^{2-} anion, which produces no shielding effect; hence, all the vacant sites on the surface are usable for the incorporation of Ni^{2+}. The situation is rather different for the case of WO_3, as each incorporated W^{6+} ion is accompanied by three oxygen capping anions for charge compensation; the shielding effect produced by these capping anions prevents some of the neighboring vacant sites on anatase from being incorporated by other tungsten ions, and accordingly the dispersion capacity of WO_3 on TiO_2 is only 4.91 W^{6+}/nm^2 (TiO_2). It can be proved by calculation that upon WO_3 reaching its dispersion capacity, the oxygen anions accompanied with the incorporated W^{6+} ions form a close-parked monolayer on the surface of anatase with some still unoccupied vacant sites underneath. Noticeably, as discussed above for the case of NiO on TiO_2, upon NiO reaching its dispersion capacity all the surface vacant sites are occupied by the incorporated Ni^{2+}, and the capping oxygen anions form an epitaxial arrangement (not close-packed) on the surface of anatase and enroll into the formation of an octahedral coordination environment for the incorporated Ni^{2+} ions. The consideration that each incorporated cation is accompanied by a stoichiometric number of capping anion(s). e.g., $1O^{2-}$ for M^{2+}, $2O^{2-}$ for M^{4+} etc., is one of the basic assumptions of the incorporation model for the sake of charge compensation (4), which has nothing to do with the formal charge of the incorporated cation. In fact, it seems reasonable to consider that after all charge is shared with the bulk, each cation is bonded by a number of anions depending on the surface structure of the support and the number of the accompanied anions; as mentioned above although there is only one O^{2-} anion come with each Ni^{2+}, the incorporated nickel ion is most probably octahedrally coordinated on the surface of anatase. Generally speaking, when the loading amount of a metal oxide is lower than its dispersion capacity, the dispersed cations might incorporate into the surface vacant sites of the support; when the loading amount exceeds its dispersion capacity, bulk-phase (crystallized) metal oxide will show up. To use the term "incorporation" in these discussions is for the purpose of emphasizing the importance of the surface vacant sites for the dispersion of the metal oxide on support. It does not mean that the incorporated cations have to sit geometrically into the sites; in fact, their location should depend on their bonding lengths and angles with the neighborhood oxygen anions established.

Characterization of the Binary Oxide Systems Supported on Anatase

Shown in Fig. 8 are TPR profiles of the NiO/TiO_2 samples. Mainly only one peak around 470 K is observed for samples with NiO loading below its dispersion capacity, i.e., curve

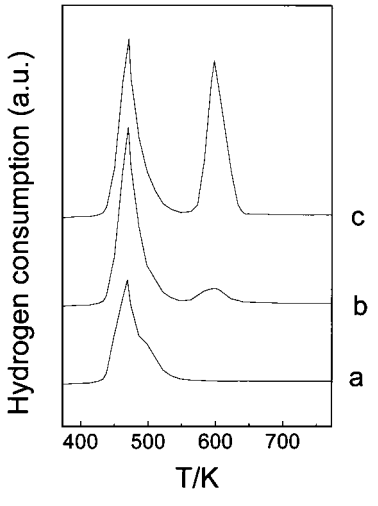

FIG. 8. TPR profiles of the reduction of NiO in NiO/TiO_2 samples: (a) $Ni(2.9)/TiO_2$, (b) $Ni(7.2)/TiO_2$, and (c) $Ni(11.9)/TiO_2$.

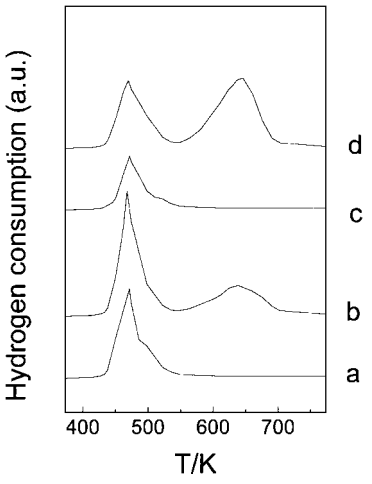

FIG. 9. TPR profiles of the reduction of NiO in $NiO/WO_3–TiO_2$ samples: (a) $Ni(3.0)/W(3.0)–TiO_2$, (b) $Ni(6.0)/W(3.0)–TiO_2$, (c) $Ni(1.7)/W(4.8)–TiO_2$, and (d) $Ni(4.8)/W(4.8)–TiO_2$.

a of the $Ni(2.9)/TiO_2$ sample (the small shoulder peak in the spectrum next to the main peak might result from a two-step reduction of the supported nickel oxide or the reduction of the anatase induced by the reduction of nickel oxide; the origin of the shoulder peak is not discussed in detail as it is not critical for the discussion of this paper); another peak around 598 K appears in samples with NiO loading exceeds its dispersion capacity, i.e., curves b and c of the $Ni(7.2)/TiO_2$ and $Ni(11.9)/TiO_2$ samples, respectively. It seems reasonable to attribute the peaks at ~470 and ~598 K to the reduction of the dispersed NiO and the supported crystalline NiO, respectively, as the existence of the bulk-phase NiO in the sample has been proved by XRD. The results are similar to those of the CuO/TiO_2 system reported elsewhere (38).

The TPR profiles of the $NiO/WO_3–TiO_2$ samples, i.e., NiO supported on WO_3-modified anatase, are shown in Fig. 9. For the $Ni(3.0)/W(3.0)–TiO_2$ (profile a) and $Ni(1.7)/W(4.8)–TiO_2$ samples (profile c), basically only one peak around 470 K is observed, which is assigned to the highly dispersed NiO species on the surface of the above two WO_3-modified anatase supports, as it is known that on the $W(3.0)–TiO_2$ support only 3.0 sites/nm^2 of TiO_2 are occupied by W^{6+} cations and there are about 3.98 sites/nm^2 of TiO_2 available for the incorporation of Ni^{2+}, and in addition, the absence of TPR peak for the WO_3/TiO_2 samples at temperatures lower than 750 K has been confirmed by complementary experiments. As can be seen from Fig. 9, for the cases of the $Ni(6.0)/W(3.0)–TiO_2$ and $Ni(4.8)/W(4.8)–TiO_2$ samples (profiles b and d, respectively), in addition to the peak around 470 K, another peak around 640 K is observed, which is attributed to the reduction of the crystalline NiO phase that has been detected by XRD analysis as shown in Table 3. Attention has been paid to the dispersion of NiO on the WO_3-modified anatase $W(4.8)–TiO_2$. The presence of a TPR peak around 470 K in the $Ni(1.7)/W(4.8)–TiO_2$ and $NiO(4.8)/W(4.8)–TiO_2$ samples (profiles c and d, respectively) points to the fact that NiO can be dispersed on $W(4.8)–TiO_2$, which was prepared by modifying the surface of anatase with WO_3 at a loading of 4.8 W^{6+}/nm^2 of TiO_2; i.e., the oxygen ions accompanying the incorporated W^{6+} have already formed a nearly closed-packed monolayer on the surface of the modified anatase. Noticeably, XRD results (Table 3) indicate no other species besides crystalline anatase in the $Ni(1.7)/W(4.8)–TiO_2$ sample, and XRD quantitative analysis has further indicated that the dispersion capacity of NiO on $W(4.8)–TiO_2$ is about 2.0 Ni^{2+}/nm^2 of TiO_2. For the WO_3-modified anatase support $W(4.8)–TiO_2$, 4.80 sites/nm^2 of TiO_2 of the surface vacant sites on anatase (a total of 6.98 sites/nm^2 (TiO_2)) have already been occupied by the incorporated W^{6+} ions with 2.18 sites/nm^2 of TiO_2 remaining vacant; the value is in good agreement with the measured dispersion capacity of NiO on $W(4.8)/TiO_2$. The above results seem to suggest that upon thermal treatment at 773 K, supported Ni^{2+} cations can migrate across the oxygen capping layer and incorporate into those unoccupied surface vacant sites. Similar results have been obtained in our studies on the $NiO/MoO_3–ZrO_2$ system reported elsewhere (40).

The dispersion of WO_3 on NiO-modified anatase has also been investigated for comparison. TPR profiles of the two NiO-modified supports, i.e., $Ni(4.8)–TiO_2$ and $Ni(6.4)–TiO_2$, have shown only a hydrogen consumption peak around 470 K corresponding to the reduction of highly dispersed NiO species. The results are consistent with the fact that the loading amounts of NiO in the above two modified supports are lower than its dispersion capacity on anatase. Shown in Fig. 10 are the TPR profiles of samples that have various WO_3 loadings prepared by the impregnation of WO_3 on the above modified supports, i.e., (a) $W(4.4)/Ni(4.8)–TiO_2$, (b) $W(2.4)/Ni(4.8)–TiO_2$, and (c) $W(3.0)/Ni(6.4)–TiO_2$, the common feature of these profiles is that two peaks, one around 478 K and the other around

TABLE 3

XRD Results of TiO_2-Supported Binary Oxide Systems

Sample	Characteristic XRD peaks			
	TiO_2	WO_3	NiO	Other
$Ni(3.1)–W(6.0)/TiO_2$	Yes	No	No	No
$Ni(6.0)–W(3.1)/TiO_2$	Yes	No	No	No
$Ni(3.6)–W(3.7)/TiO_2$	Yes	No	No	No
$Ni(3.0)/W(3.0)–TiO_2$	Yes	No	No	No
$Ni(6.0)/W(3.0)–TiO_2$	Yes	No	Yes	No
$Ni(1.7)/W(4.8)–TiO_2$	Yes	No	No	No
$Ni(4.8)/W(4.8)–TiO_2$	Yes	No	Yes	No
$W(4.4)/Ni(4.8)–TiO_2$	Yes	No	No	No
$W(2.4)/Ni(4.8)–TiO_2$	Yes	No	No	No
$W(3.0)/Ni(6.4)–TiO_2$	Yes	No	No	No

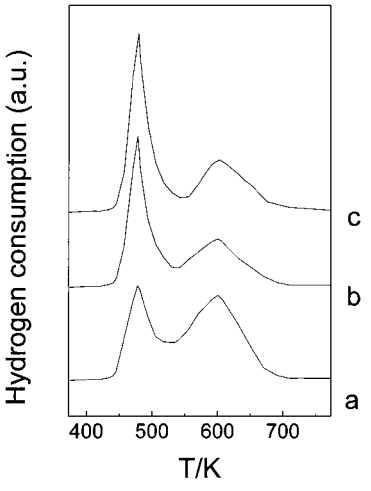

FIG. 10. TPR profiles of the reduction of NiO in WO_3/NiO–TiO_2 samples: (a) W(4.4)/Ni(4.8)–TiO_2, (b) W(2.4)/Ni(4.8)–TiO_2, and (c) W(3.0)/Ni(6.4)–TiO_2.

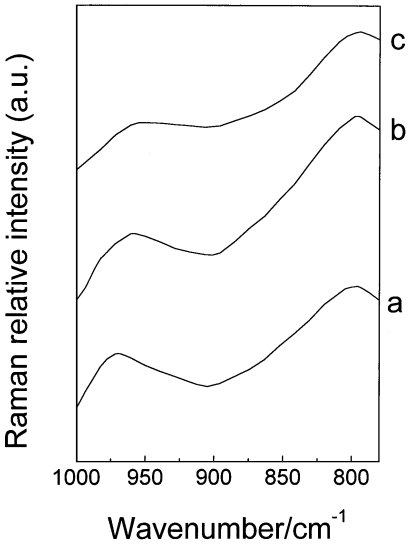

FIG. 12. Raman spectra of the NiO–WO_3/TiO_2 samples: (a) Ni(3.1)–W(6.0)/TiO_2, (b) Ni(6.0)–W(3.1)/TiO_2, and (c) Ni(3.6)–W(3.7)/TiO_2.

600 K, can clearly be seen. Complementary XRD experiments have proved that there is neither crystalline WO_3 nor crystalline NiO nor any other bulk-phase species besides TiO_2 in these samples. Consequently, the most plausible explanation for the above results is that upon addition of W^{6+} at least part of the incorporated Ni^{2+} cations are replaced with the formation of a new surface species by the interaction between highly dispersed WO_3 and NiO species; as discussed in the following paragraphs the reduction peak at ~600 K can be assigned to the contribution of this new species.

TPR profiles of NiO–WO_3/TiO_2 samples prepared by the coimpregnation of Ni^{2+} and W^{6+} cations on anatase are shown in Fig. 11. The unique feature of these profiles is that only one hydrogen consumption peak around 603 K has been observed. Taking into consideration that the loading amounts of the two oxide species are rather high and XRD results have shown the absence of any crystalline phase besides anatase in these samples, the conclusion that a new surface species formed by the interaction between the supported W^{6+} and Ni^{2+} species can be derived. In fact, similar results have been reported by Scheffer *et al.*, in their studies on alumina-supported NiO–WO_3 samples (15).

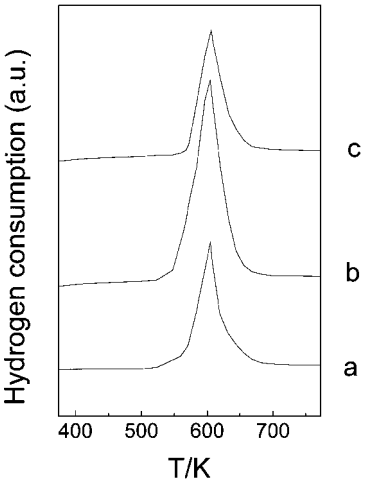

FIG. 11. TPR profiles of the reduction of NiO in NiO–WO_3/TiO_2 samples: (a) Ni(3.1)–W(6.0)/TiO_2, (b) Ni(6.0)–W(3.1)/TiO_2, and (c) Ni(3.6)–W(3.7)/TiO_2.

To get a deeper insight into the possible existence of the new surface species, Raman and DRS spectra of the above three samples are measured and shown respectively in Fig. 12 and Table 1. The two Raman peaks around 970 and 794 cm^{-1} in Fig. 12 are attributed to the contributions of the highly dispersed WO_3 species and the anatse support, respectively (26, 27). It is well known that the Raman spectrum is rather sensitive in detecting the existence of a crystalline WO_3 phase, and the absence of any crystalline WO_3 in Fig. 12 seems to strongly suggest that the supported W^{6+} species are highly dispersed on the surface with the formation of a new surface interaction species, as the WO_3 content in the Ni(3.01)–W(6.02)/TiO_2 sample is already beyond its dispersion capacity on anatase.

DRS of the above three samples also supports the above conclusion. As shown in Table 1 two absorption bands around 470 and 665 nm are observed in DRS. The ~665 nm band attributed to the dispersed Ni^{2+} surface species has also been detected in the NiO/TiO_2 samples with no bulk NiO phase detected. It has been reported that crystalline $NiWO_4$ has an adsorption band at 450 nm (15), and neither WO_3 nor anatase-supported WO_3 has absorption bands between 400 and 800 nm; thus the absorption band around 470 nm should be attributed to the contribution of the new surface species formed by the interaction of the supported W^{6+} and Ni^{2+} species discussed above.

CONCLUSIONS

(1) For single oxide supported on anatase, both nickel oxide and tungsten oxide can be highly dispersed on the surface of the support with dispersion capacities of 6.65 and 4.85 cations/nm^2 (TiO_2) for NiO and WO_3, respectively. The results are consistent with the expectations of the incorporation model, i.e., the vacant sites on the (001) plane perferentially exposed on the surface of anatase are used for the incorporation of the dispersed metal cations.

(2) For the anatase-supported binary oxide systems, the addition sequence of the oxide species is critical on the surface states of the supported oxide samples, namely:

(a) NiO can be dispersed on WO_3-modified anatase by incorporating into the residual vacant sites on the WO_3-modified support, and the measured dispersion capacity of NiO is also consistent with the value evaluated by the incorporation model.

(b) On NiO-modified anatase, supported W^{6+} cations can replace part of the incorporated Ni^{2+} cations with the formation of a new surface species highly dispersed on the surface of the support; similar surface species can also be formed by the coimpregnation of W^{6+} and Ni^{2+} species on anatase, i.e., in the NiO–WO_3/TiO_2 samples investigated.

ACKNOWLEDGMENTS

The authors appreciate the special grant from the Ministry of Education of China for doctoral studies.

REFERENCES

1. Knözinger, H., *Adv. Catal.* **25**, 184 (1976).
2. Massoth, F. E., *Adv. Catal.* **27**, 265 (1978).
3. Xie, Y. C., and Tang, Y. Q., *Adv. Catal.* **37**, 1 (1990).
4. Chen, Y., and Zhang, L. F., *Catal. Lett.* **12**, 51 (1992).
5. Rymer, G. T., Bridge, J. M., and Tomlinson, J. R., *J. Phys. Chem.* **15**, 157 (1962).
6. Schiavello, M., LoJacono, M., and Cimino, A., *J. Phys. Chem.* **71**, 1051 (1971).
7. Thomas, R., and Moulijn, J. A., *J. Mol. Catal.* **15**, 157 (1982).
8. Bailey, G. C., *Catal. Rev.* **3**, 37 (1969).
9. Imanari, M., Watanabe, Y., Matsuda, S., and Nakajima, F., "Proceedings, 7th International Congress on Catalysis, Tokyo, 1980" (T. Seiyama and K. Tanabe, Eds.), p. 41. Elsevier, Amsterdam, 1981.
10. Grange, P., *Catal. Rev.-Sci. Eng.* **21**, 135 (1980).
11. Frank, J. P., and Lepage, J. F., "Proceedings, 7th International Congress on Catalysis, Tokyo, 1980" (T. Seiyama and K. Tanabe, Eds.), p. 792. Elsevier, Amsterdam, 1981.
12. Weisser, O., and Landa, S., "Sulphide Catalysts, their Properties and Applications." Pergamon, New York, 1973.
13. Scheffer, B., Arnoldy, P., van Oers, E. M., de Beer, V. H. J., and Moulijn, J. A., *Appl. Catal.* **25**, 303 (1986).
14. Thomas, R., van Oers, E. M., de Beer, V. H. J., Medema, J., and Moulijn, J. A., *J. Catal.* **76**, 241 (1982).
15. Scheffer, B., Heijeinga, J. J., and Moulijn, J. A., *J. Phys. Chem.* **91**, 4752 (1987).
16. Ng, K. T., and Hercules, D. M., *J. Phys. Chem.* **80**, 2094 (1976).
17. Ostromecki, M. M., Burcham, L. J., Wachs, I. E., Ramani, N., and Ekerdt, J. G., *J. Mol. Catal. A: Chemical* **132**, 43 (1998).
18. Ostromecki, M. M., Burcham, L. J., and Wachs, I. E., J. G., *J. Mol. Catal. A: Chemical* **132**, 59 (1998).
19. Matsuda, S., and Kato, A., *Appl. Catal.* **8**, 149 (1983).
20. Jones, H. B., and Smith, R., U.S. Patent 4206038, 1980.
21. Okamoto, Y., Maezawa, A., and Imamaka, T., *J. Catal.* **120**, 29 (1989).
22. LoJacono, M., Schiavello, M., and Cimino, A., *J. Phys. Chem.* **71**, 1044 (1971).
23. Houalla, M., and Delmon, B., *J. Phys. Chem.* **84**, 2194 (1980).
24. Zhang, L. F., Lin, J. F., and Chen, Y., *J. Chem. Soc., Faraday Trans.* **88**, 497 (1992).
25. Dunitz, J. D., and Orgel, L. E., *J. Phys. Chem. Solids* **3**, 318 (1957).
26. Chan, S. S., Wachs, I. E., Murrell, L. L., Wang, L., and Hall, W. K., *J. Phys. Chem.* **88**, 5831 (1984).
27. Vuurman, M. A., Wachs, I. E., and Hirt, A. M., *J. Phys. Chem.* **95**, 9928 (1991).
28. Ramani, N. C., Sullivan, D. L., Ekerdt, J. G., Jehng, J. M., and Wachs, I. E., *J. Catal.* **176**, 143 (1998).
29. Wachs, I. E., and Murrell, L. L., *J. Catal.* **90**, 150 (1984).
30. Vuurman, M. A., and Wachs, I. E., *J. Phys. Chem.* **96**, 5008 (1992).
31. Salvati, L., Jr., Makovsky, L. E., Stencei, J. M., Brown, F. R., and Hercules, D. M., *J. Phys. Chem.* **85**, 3700 (1981).
32. Billoen, P., and Pott, G. T., *J. Catal.* **30**, 169 (1973).
33. Fung, S. C., *J. Catal.* **58**, 454 (1979).
34. Dong, L., and Chen, Y., *J. Chem. Soc., Faraday Trans.* **92**, 4589 (1996).
35. Chen, Y., Zhang, L. F., Lin, J. F., and Jin, Y. S., "Catalytic Science and Technology," p. 291. Ono Kodansha Ltd., Tokyo, 1991.
36. Chen, Y., Dong, L., Jin, Y. S., Xu, B., and Ji, W. J., *Stud. Surf. Sci. Catal.* **101**, 1293 (1996).
37. Dong, L., Jin, Y. S., and Chen, Y., *Sci. China, Ser. B* **40**, 24 (1997).
38. Xu, B., Dong, L., and Chen, Y., *J. Chem. Soc., Faraday Trans.* **94**, 1905 (1998).
39. Primet, M., Pichat, P., and Mathieu, M. V., *J. Phys. Chem.* **75**, 1216 (1971).
40. Liu, Z., and Chen, Y., *J. Catal.* **177**, 314 (1998).